Acta Pharmaceutica Sinica B 2025;15(7):3805−3818

Chinese Pharmaceutical Association
Institute of Materia Medica, Chinese Academy of Medical Sciences

Acta Pharmaceutica Sinica B

www.elsevier.com/locate/apsb
www.sciencedirect.com

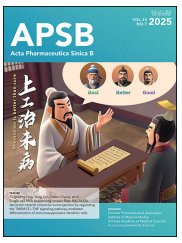

ORIGINAL ARTICLE

Polymer-assisted PD-L1 degradation and targeted photodynamic therapy synergize to suppress immunodeficient tumors

Changyong Guo[†], Shipeng He[*,†], Huaxing Shen, Wei Cong, Jinqiu Li, Yajing Ji, Wenjing Huang, Fei Gao[*], Honggang Hu[*]

School of Medicine, Institute of Translational Medicine, Shanghai Engineering Research Center of Organ Repair, Shanghai University, Shanghai 200444, China

Received 10 November 2024; received in revised form 12 January 2025; accepted 3 March 2025

KEY WORDS

Immunotherapy;
PD-L1;
Photodynamic therapy;
Protein degradation;
Polymer;
Immunogenic cell death;
Reactive oxygen species;
Cytotoxic T lymphocytes

Abstract Checkpoint blockade immunotherapy has emerged as a transformative approach in cancer treatment by activating tumor-infiltrating T cells. However, the efficacy of PD-L1 blockade is restricted in "cold" tumors, which are characterized by low immunogenicity, presenting a challenge to immunotherapy. This study introduces an innovative strategy, utilizing cathepsin-cleavable *N*-(2-hydroxypropyl) methacrylamide (HPMA) polymer-assisted combined photodynamic therapy (PDT) and PD-L1 degradation for the first time, effectively treating T cell-deficient tumors. The degradable main-chain polymer, conjugated with photosensitizer porphyrin, facilitates the accumulation of reactive oxygen species (ROS), triggering immunogenic cell death (ICD) and promoting cytotoxic T lymphocytes (CTLs) infiltration into tumors. Multivalent peptide antagonists of PD-L1 promote PD-L1 degradation in lysosomes through receptor crosslinking, overcoming the adaptive cycling of PD-L1 to the tumor cell surface. These findings demonstrate that polymer-assisted PDT and PD-L1 crosslinking degradation represent a potential novel strategy for anti-tumor immunotherapy, providing valuable tools for expanding immunotherapy applications in immunosuppressive cancers.

*Corresponding authors.
E-mail addresses: heshipeng@shu.edu.cn (Shipeng He), flyhightly@shu.edu.cn (Fei Gao), hhu66@shu.edu.cn (Honggang Hu).
[†]These authors made equal contributions to this work.

Peer review under the responsibility of Chinese Pharmaceutical Association and Institute of Materia Medica, Chinese Academy of Medical Sciences.

https://doi.org/10.1016/j.apsb.2025.05.022

1. Introduction

The interaction between the programmed cell death-1 (PD-1) receptor on T cells and programmed cell death ligand-1 (PD-L1) on cancer cells is critically important to the tumor immune evasion mechanism. Competitive blockade by immune checkpoint inhibitors targeting the PD-L1 and PD-1 interaction can activate preexisting tumor-infiltrating T cells, providing sustained suppression of cancer, and emerging as a transformative technique in tumor therapy[1-4]. However, the efficacy of PD-L1 blockade is limited in "cold" tumors lacking T cell infiltration and exhibiting low immunogenicity[5,6]. Consequently, transforming "cold" tumors into "hot" tumors with anti-tumor T cell immunity poses a significant challenge for immunotherapy[7]. PD-L1 blockade therapy can synergize with chemotherapy[8] or oncolytic therapy[9], inducing immunogenic cell death (ICD) in tumor cells. Unlike most cytotoxic chemotherapeutic drugs, photodynamic therapy (PDT) using photosensitizers (PSs) can lead to the accumulation of intracellular reactive oxygen species (ROS), triggering ICD effects, promoting the infiltration of cytotoxic T lymphocytes (CTLs) into tumors, and eliciting an immune response[10-14]. Additionally, the photochemical reactions generated by PDT can directly damage tumor cells, making it an ideal adjunctive strategy to enhance the efficacy of immunotherapy[15,16]. However, PS drugs, being small-molecule agents, exhibit non-targeted effects, potentially entering normal tissues and causing adverse side effects[17]. The 2nd-generation degradable *N*-(2-hydroxypropyl) methacrylamide (HPMA) represents an ideal delivery vehicle for small-molecule drugs[18-20]. Its copolymers can conjugate multiple drugs, forming nanoparticles that leverage the enhanced permeability and retention (EPR) effect, thereby enhancing the targeted delivery capability of these drugs[19,21-23]. This provides a novel strategy for improving the tumor-targeting capabilities of PS drugs.

In the treatment of tumors with anti-PD-L1 antibodies (α-PD-L1), despite the formation of a conformational blockade on the tumor cell membrane against PD-L1, the extracellular expression of PD-L1 can still be maintained. This is attributed to the active recycling of PD-L1 after binding with α-PD-L1, leading to its reemergence on the cell surface[24,25]. Studies indicated that inducing receptor crosslinking on the cell membrane can lead to the ligand's targeting transport towards lysosomes. Through this receptor crosslinking strategy, it prompts the degradation of PD-L1 in lysosomes[26,27], thereby inhibiting the circulation of PD-L1 and enhancing the T cell immune response against tumors. HPMA copolymers are considered ideal materials for developing PD-L1-binding peptide crosslinkers[28]. Additionally, envisioning linear HPMA copolymers with multiple PD-L1-binding peptides may be more advantageous for receptor crosslinking, as the random coil conformation of peptides facilitates better presentation of the targeting moiety, and the multivalency of coupled ligands allows simultaneous crosslinking of multiple PD-L1 receptors[25,29]. This strategy, which directly induces PD-L1 degradation, shows a tendency for quicker reduction of PD-L1 levels compared to certain nanosystems that regulate PD-L1, along with superior material biocompatibility[30-33].

In this study, we devised a strategy based on cathepsin-cleavable HPMA polymer-conjugated PSs, porphyrin (Ce6). This strategy ingeniously integrates the advantages of PDT, PDT-induced ICD, and PD-L1 degradation, effectively treating tumors lacking T cells. The degradable HPMA copolymer−porphyrin conjugate (HPC) facilitates the accumulation of the immunogenic drug PSs in tumors, induces PDT effects under near-infrared light, and robustly induces ICD, promoting T cell infiltration. The degradability of the polymer backbone is achieved by introducing a peptide sequence (GGFGKGFGG) susceptible to tissue protease degradation[34]. The multivalent conjugate of multiple PD-L1 antagonistic peptides (NYSKPTDRQYHF) on the degradable HPMA copolymer[35], termed HPAP, leads to the cross-linking of PD-L1 receptors, internalizes into lysosomes, and efficiently degrades, preventing PD-L1 from further cycling. Following the combined administration of HPC and HPAP, PDT under light exposure stimulates anti-tumor immunity, activates T cells recruited by HPC, enhances immune responses, and effectively inhibits tumor growth.

2. Materials and methods

2.1. General methods

Methanol (MeOH), dichloromethane (DCM), *N*,*N*-dimethylformamide (DMF), *N*,*N*-diisopropylethylamine (DIEA), *N*,*N*′-diisopropylcarbodiimide (DIC), 1-hydroxybenzotriazole (HOBT), trifluoroacetic acid, formic acid, dialysis bags were purchased from Titan Technology Co., Ltd., (Shanghai China). *N*-(2-Hydroxypropyl) methacrylamide, 4,4′-azobis (4-cyanovaleric acid) (V501), 4-cyano-4-(phenylcarbonothioylthio) pentanoic acid (CAT), trifluoroacetic acid (TFA) and trifluoroethanol (TFE) were purchased from Aladdin Technology Co., Ltd. (Shanghai China). Protein immunoblotting secondary antibodies, reactive oxygen species assay kit, Western blot primary, and secondary antibody dilution solutions, nuclear-staining reagent (DAPI), and CCK-8 assay kit were purchased from Beyotime Biotechnology (Shanghai China). Alexa Fluor 594 was purchased from Abbkine Biotechnology Co., Ltd. (Wuhan China). 1640 medium, trypsin, penicillin−streptomycin, and chemiluminescent secondary antibodies were purchased from Sangon Biotech Co., Ltd. (Shanghai China). PD-L1 mouse primary antibody was purchased from Abcam. Protein mark, $CD8^+$, $CD4^+$, $CD86^+$, $CD80^+$, and $Foxp3^+$ flow cytometry antibodies were purchased from Becton, Dickinson and Company (US). TNFα, IL-6, IFN-γ ELISA kits, and cell apoptosis assay kits were purchased from MultiSciences Technology Co., Ltd. (Shanghai China). Electrophoresis buffer and transfer buffer were purchased from Epizyme Biomedical Technology Co., Ltd. (Shanghai China). The serum was purchased from Gibco (Brazil South America). Detailed synthesis routes and characterization of conjugated HPC and HPAP nanoparticles can be found in Supporting Information Figs. S1 and S2.

2.2. Cell culture

The 4T1 cell line was obtained from the Chinese Academy of Sciences and cultured in RPMI 1640 medium without HEPES (obtained from Sangon Biotech Co., Ltd.), supplemented with 1% penicillin and streptomycin and 10% fetal bovine serum. The cells were seeded in RPMI 1640 medium in 96-well or 6-well plates and cultured at 37 °C with 5% CO_2.

2.3. Cell toxicity study

4T1 cells were seeded in 96-well plates at a density of 1×10^4 cells per well and incubated for 24 h before adding the test nanoparticles. Different treatment groups including PBS, Ce6-dark, Ce6-light, HPC-dark, and HPC-light were set up to

investigate the cell toxicity of the nanoparticles. After 24 h incubation with the test nanoparticles, CCK-8 was added to the culture medium and further incubated for 2 h. The absorbance at 450 nm was measured to assess cell viability. Finally, the data from each group was analyzed using GraphPad Prism 8.

2.4. Cellular internalization

To elucidate the mechanisms of cellular internalization, 4T1 cells were plated at a seeding density of 5×10^5 cells per well in 6-well plates. These cells were subsequently exposed to various treatments, including PBS, Ce6, HPAP, and HPC, to assess differences in cellular uptake. Post-incubation, flow cytometry was utilized to quantitatively analyze the internalization of these nanoparticles by the 4T1 cells. Furthermore, for detailed subcellular localization analysis, the cells were seeded onto glass-bottom culture dishes and subjected to staining with specific lysosomal and mitochondrial probes. This preparatory work was followed by use of laser scanning confocal microscopy (Olympus, fv3000 Japan) to visually assess the uptake and intracellular trafficking of the drugs. Finally, the data from each group was analyzed using GraphPad Prism 8.0.

2.5. The generation of ROS

To quantitatively evaluate the induction of reactive oxygen species (ROS) in 4T1 cells, an ROS assay kit was employed. Initially, the cells were cultured in 6-well plates at a density of 5×10^5 cells per well, followed by a 24-h incubation period to ensure adherence and stable growth. Subsequent treatments involved administering HPC-dark and HPC-light, with a set of cells receiving no treatment to act as the baseline control. The cells were treated with DCFH-DA (Beyotime) according to the manufacturer's protocol. The generation of ROS was subsequently measured using flow cytometry (Beckman colter, CytoFLEX US).

2.6. Pharmaceutical agent release

A quantity of the pharmaceutical HPC (1 mg) was dissolved in 4 mL of PBS. This solution was then introduced into a dialysis bag and subjected to incubation at 37 °C for varying durations of 0.5, 1, 2, 4, 8, and 16 h. Consequent to each specified incubation period, aliquots were extracted for analysis. The absorbance characteristic of the drug was quantitatively assessed employing Ultraviolet (UV) spectrophotometry (Thermo, Biomate 160 US).

2.7. Analysis by electron microscopy

2 mg of HPMA and HPC were dissolved in 2 mL of ultrapure water. This solution was then agitated continuously for 4 h. After this mixing period, a 0.5 mL aliquot of the solution was applied to a copper grid, allowed to stand for 24 h, and then subjected to staining with uranyl acetate. Following a 12 h staining interval, the samples were imaged using a transmission electron microscope (JEM-2010 TEM, Japan). In a parallel experiment focusing on cellular response, 5×10^5 4T1 cells were seeded into culture dishes and treated with 0.5 μmol/L of the HPAP drug. After a 4 h incubation period with the drug, the cells were detached employing a cell scraper, fixed with a specialized electron microscopy fixative, stained with uranyl acetate and subsequently imaged using a biological transmission electron microscope (HITACHI HT7800, Japan). Additionally, 2 mg of HPMA and HPC were each dissolved in 2 mL of anhydrous ethanol, incubated for 15 min, and then dispensed dropwise onto a silicon wafer. Following a 12 h drying period, the samples were coated with gold *via* sputtering and imaged utilizing a scanning electron microscope (SU1510 SEM, Japan).

2.8. Apoptosis assessment

The cells were initially seeded at a density of 5×10^5 cells per well in the cultivation and treatment of 4T1 cells in a 6-well plate and incubated for 24 h. After achieving a fusion rate of approximately 70%, various drugs were added to each group and incubated for another 24 h. The cells were then collected and stained using V-FITC and propidium iodide (PI) according to the manufacturer's instructions. Flow cytometry was used to analyze the cells. Finally, the data from each group was analyzed using GraphPad Prism 8.0.

2.9. Protein expression analysis

To detect the expression of PD-L1 protein in 4T1 cells, Western blotting was used to measure the expression levels of PD-L1. 4T1 cells were seeded in a 6-well plate at a density of 5×10^5 cells per well. After 24 h of incubation, the cells were divided into different groups, PBS, HPAP, (HPC + HPAP)-dark, and (HPC + HPAP)-light groups. The cells were treated for 24 h, and then the cell membrane proteins were extracted for analysis to determine the degradation effect of the drug on the PD-L1 protein.

2.10. Ex vivo immune factor induction experiment

4T1 and RAW264.7 cells were cultured at an initial seeding density of 5×10^5 cells well within 6-well plates. After a 12 h incubation period in standard culture media, the cells were subjected to various treatment conditions, including PBS, HPAP, HPC-dark, HPC-light, (HPC + HPAP)-dark, and (HPC + HPAP)-light groups, for an additional incubation period of 24 h. Subsequent to these treatments, for the intricacies of immune response analysis, culture media supernatants were harvested and assayed for the presence of cytokines TNFα, IL-6, and IFN-γ employing an ELISA protocol detailed by the manufacturer (MultiSciences Biotech Co., Ltd. China.).

2.11. ICD induction in vitro

4T1 cells were seeded at a density of 5×10^5 cells in a 6-well plate and cultured in media for 12 h. After that, PBS, HPC-dark, HPC-light, HPAP, (HPC + HPAP)-dark, and (HPC + HPAP)-light treatment groups were added to the media. The cells were then incubated for 24 h. In the ICD induction experiment, the supernatant from the media was collected and analyzed for ATP and HMGB-1 using an ELISA kit. 2×10^5 4T1 cells were seeded in a glass-bottom dish (Solarbio, Beijing, China) and incubated with calreticulin (CRT) antibody. Then, the cells were stained with Alexa Fluor 594 (Abbkine Scientific Co., Ltd., China) secondary antibody. The drug-induced CRT expression in the cells was observed using laser confocal microscopy (Olympus, fv3000, Japan).

2.12. Animal experiment operation and immune stimulation in vivo

The animal model for breast cancer employed female BALB/c mice aged 6 weeks, weighing between 18 and 21 g, sourced from

the Animal Facility of the Shanghai University School of Translational Medicine. All experimental procedures were executed according to the protocols approved by the Shanghai University School of Translational Medicine Animal Care and Use Committee. 2×10^5 4T1 cells were implanted into the right hind limb of each mouse in the study on BALB/c tumor-bearing mice. The study encompassed a control group (treated with physiological saline) and several experimental groups (HPAP, HPC-dark, HPC-light, (HPC + HPAP)-dark, and (HPC + HPAP)-light). Administration of the drug commenced once the tumor reached a volume of 100 mm^3. Light exposure was performed every two days (using 660 nm laser irradiation with a power density of 250 mmol/L/cm^2 for 6 min, totaling 90 J/cm^2 of light intensity). The weight of the mice and the volume of their tumors were measured every alternate day. Following five doses of drug administration, the mice were euthanized *via* cervical dislocation. The heart, liver, spleen, lungs, and kidneys were harvested for hematoxylin and eosin (H&E) staining to assess any potential organ damage induced by the drug. Additionally, tumor tissues from each group underwent PD-L1 immunofluorescence staining, H&E staining, and Ki67 immunohistochemistry for further analysis. For cellular analysis, tumor or lymphatic tissues were excised, with approximately 1 g of each tissue processed under sterile conditions. Tissue samples were minced and subjected to enzymatic digestion using type IV collagenase for 1 h at 37 °C with continuous agitation. Following dispersion, tissues were passed through a cell strainer to obtain a cell suspension, which was then filtered through a 70 μm strainer to remove aggregates. The suspension was washed with PBS, and single cells were collected and cooled on ice. Post PBS washing and centrifugation at 1400 rpm for 5 min at 4 °C, the supernatant was discarded. Lymphocytes were isolated using the TBD LTS1092PK mouse spleen lymphocyte separation reagent kit, with the cell suspension further filtered to eliminate debris. Cells were resuspended in PBS, counted, and adjusted to 1×10^5 cells in 500 μL for staining with $CD80^+/CD86^+$ primary antibodies for lymphocytes, $CD8^+/CD4^+$ and $Foxp3^+/CD4^+$ for tumor cells, respectively. Each staining was followed by incubation at room temperature for 30 min, washing, and resuspension in PBS for flow cytometric analysis (Beckman colter, CytoFLEX, US).

3. Results and discussion

3.1. Design rationale

The combination of PSs and PD-L1 binding peptides using cathepsin-cleavable HPMA polymers represents a promising strategy for effectively treating T cell-defective tumors by synergizing the benefits of PDT and PD-L1 degradation. Initially, the HPMA copolymer is linked to the PSs to form the HPC nanoparticles, which enhances the accumulation of the immunogenic drug PSs in the tumor. Upon exposure to near-infrared light, HPC induces a PDT effect, resulting in the lysis and apoptosis of tumor cells. Additionally, under near-infrared light irradiation, PSs trigger the release of antigen-inducing substances such as ATP, HMGB1, and CRT, which serve as antigens and are presented to dendritic cells (DCs). In response, DCs release immune factors TNFα and IL-6, promoting DC maturation and antigen presentation to T cells. This activation of the immune system's $CD8^+/CD4^+$ cytotoxicity induces a robust response against tumor cells. Overall, HPC holds considerable potential for comprehensive treatment of T cell-defective tumors by leveraging the PSs. The use of HPAP nanoparticles, formed by coupling PD-L1 antagonistic peptides with degradable HPMA copolymers, has shown great potential in improving T-cell activity and preventing tumor cells from evading immune surveillance. By targeting PD-L1 on the tumor cell membrane and employing a crosslinking internalization method to facilitate the internalization and degradation of PD-L1, HPAP effectively enhances the immune response of T cells and facilitates tumor regression. The combined application of HPAP and HPC can be used as a complementary approach to tumor immunotherapy, providing a new strategy for the treatment of tumors (Fig. 1).

3.2. In vitro characterization

HPC and HPAP, synthesized *via* one-step reversible addition−fragmentation chain transfer (RAFT) polymerization, are degradable and exhibit narrow polydispersity. The detailed synthesis methods were illustrated and characterized in Figs. S1 and S2. The size of nanoparticles and the zeta potential are critical factors for assessing the stability and effectiveness of nanoparticle-based anticancer drug delivery systems. Therefore, transmission electron microscopy (TEM) and Malvern particle size analyzer were used to test the size and zeta potential of the nanoparticles. TEM analysis confirmed the linear shape of HPMA, a cathepsin-cleavable peptide material (Fig. 2A), while the hybrid material HPC had a hydrodynamic diameter of approximately 200 nm (Fig. 2B). The scanning electron microscopy (SEM) results revealed that HPMA exhibited a linear morphology, while HPAP displayed a classical spherical shape (Supporting Information Fig. S3A and S3B). Full-wavelength scanning of HPC and Ce6 showed that the main absorption peaks of both nanoparticles were similar, indicating successful Ce6 loading (Fig. 2C). Dynamic light scattering (DLS) measurements were used to evaluate the size and charge changes of the nanoparticle HPC before and after successful encapsulation (Fig. 2D). After the successful loading of Ce6, the surface charge of HPMA decreased from +4.7 to +1.9 mV for HPC (Fig. 2E), indicating a decrease in potential after Ce6 loading. These results demonstrated the successful synthesis of the nanoparticle and drug loading systems, with a nanoparticle size of approximately 200 nm and a positive potential of +1.9 mV, showing excellent Ce6 delivery capabilities.

Furthermore, the Ce6 release in the presence and absence of cathepsins was also investigated. The results showed that in the presence of cathepsins, cumulative drug release reached 75% after 72 h (Fig. 2F). In contrast, Ce6 release was only 34% in the absence of cathepsins, indicating that the drug exhibited a better release profile in the presence of proteases. The intracellular targeting of HPAP to cell lysosomes was also validated through biological TEM, indicating the presence of HPAP in cellular lysosomes (Fig. 2G).

3.3. In vitro activities of HPC and HPAP

Cytotoxicity is the fundamental condition for evaluating drug effects[36]. Therefore, a cell counting kit-8 (CCK-8) assay was performed to evaluate the cytotoxicity of Ce6 and HPC on 4T-1 cells. The cells were seeded in a 96-well plate and incubated with predetermined concentrations of HPC and HPAP in darkness for 24 h. Subsequently, the cells were irradiated with a 660 nm wavelength laser. The results showed that the half maximal inhibitory concentration (IC_{50}) of the HPC-dark treatment group decreased to 70.03 μmol/L (Fig. 3A), while the IC_{50} of HPC under

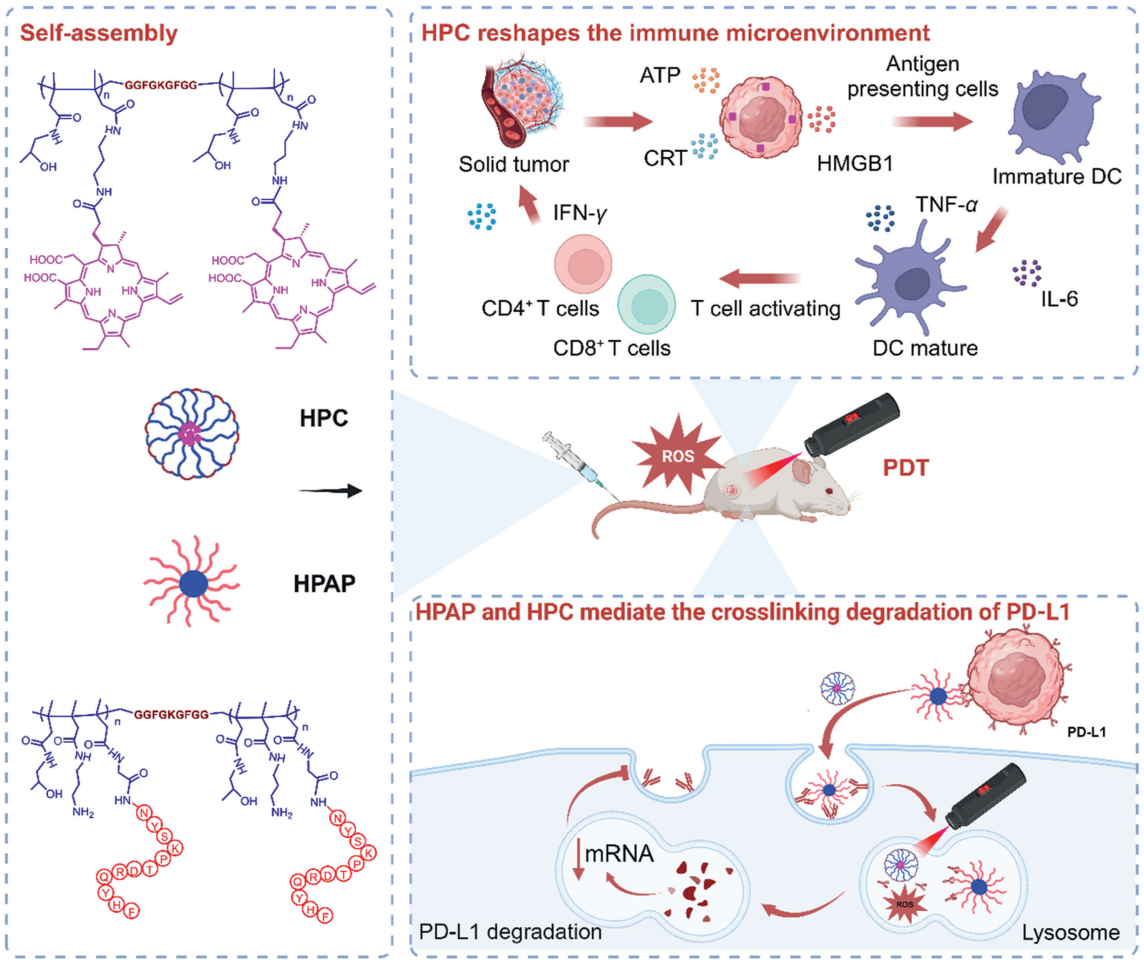

Figure 1 Conceptual illustration of the HPC and HPAP nanosystem for combined photodynamic and immunotherapy.

light conditions was 0.62 μmol/L (Fig. 3B), indicating a nearly 112-fold difference in toxicity between light and dark conditions. The IC_{50} of Ce6 under light conditions was 1.13 μmol/L (Fig. 3C). In comparison, the Ce6-dark treatment group showed an IC_{50} value of 98.83 μmol/L (Fig. 3D). However, both HPMA and HPAP exhibit nontoxic properties, even at elevated concentrations (Fig. S3C and S3D). These findings suggest that the HPC exhibited a slight improvement in cell toxicity compared to the prototype drug Ce6 at the irradiation condition with 660 nm. Additionally, we evaluated the production rate of ROS in 4T-1 cells at different drug concentrations, using different concentrations of HPC and HPAP to treat the cells. The results indicated HPC exhibited a remarkably high ROS generation rate of 93.32% under light conditions at a concentration of 2.0 μmol/L, while the dark treatment group had a ROS generation rate of only 41.15% at the same concentration. Overall, the results demonstrated that HPC had a high ROS generation rate and exerted potent cytotoxic effects on tumor cells under light conditions (Fig. 3E and F).

To further investigate the cytotoxicity under different drug concentrations, flow cytometry was performed to analyze the cell apoptosis. The findings indicated that, at a concentration of 0.5 μmol/L, the apoptotic rate for (HPC + HPAP)-dark was relatively modest, measuring 19.07%. Notably, the data illustrated a peak apoptosis rate of 50.69% for HPC-light at a concentration of 2.0 μmol/L, whereas the (HPC + HPAP)-light combination exhibited a heightened maximum apoptosis rate of 68.89% (Fig. 3G and H). The apoptosis experiment underscored a more pronounced cellular apoptotic effect under (HPC + HPAP)-light conditions. In addition, the cell cycle assay indicated that 4T-1 cells were arrested in the radiation-sensitive G1/G0 phase under (HPC + HPAP)-light conditions, while in the dark-treated group, the cell cycle arrest occurred in the S phase (Supporting Information Figs. S4 and S5).

3.4. Subcellular localization and degradation effect on PD-L1

Cellular uptake and internalization pathways are crucial for the delivery efficiency and biological utilization of nanocarriers, thus, the subcellular localization of HPC and HPAP was further investigated. In the cellular uptake study, culture dishes were supplemented with 0.5 μmol/L Rhodamine B-modified HPAP (RhodamineB−HPAP) (Fig. S2) and HPC. The results showed that HPC accumulated highly in lysosomes and mitochondria (Fig. 4A), with mitochondrial stress inducing cell apoptosis. Rhodamine B-HPAP targeted the lysosomes of targeted cells and degraded overexpressed PD-L1 protein within the cells. Flow cytometry confirmed the cellular uptake of HPC and Ce6 at the same concentration, demonstrating that HPC exhibited stronger cellular uptake than Ce6 alone (Fig. 4B and C). These findings demonstrate the efficient cellular uptake and subcellular targeting ability of HPC. Furthermore, laser confocal microscopy confirmed the degradation effect of composite HPAP on PD-L1 protein. The results showed that administration of 10 μmol/L polymer HPAP

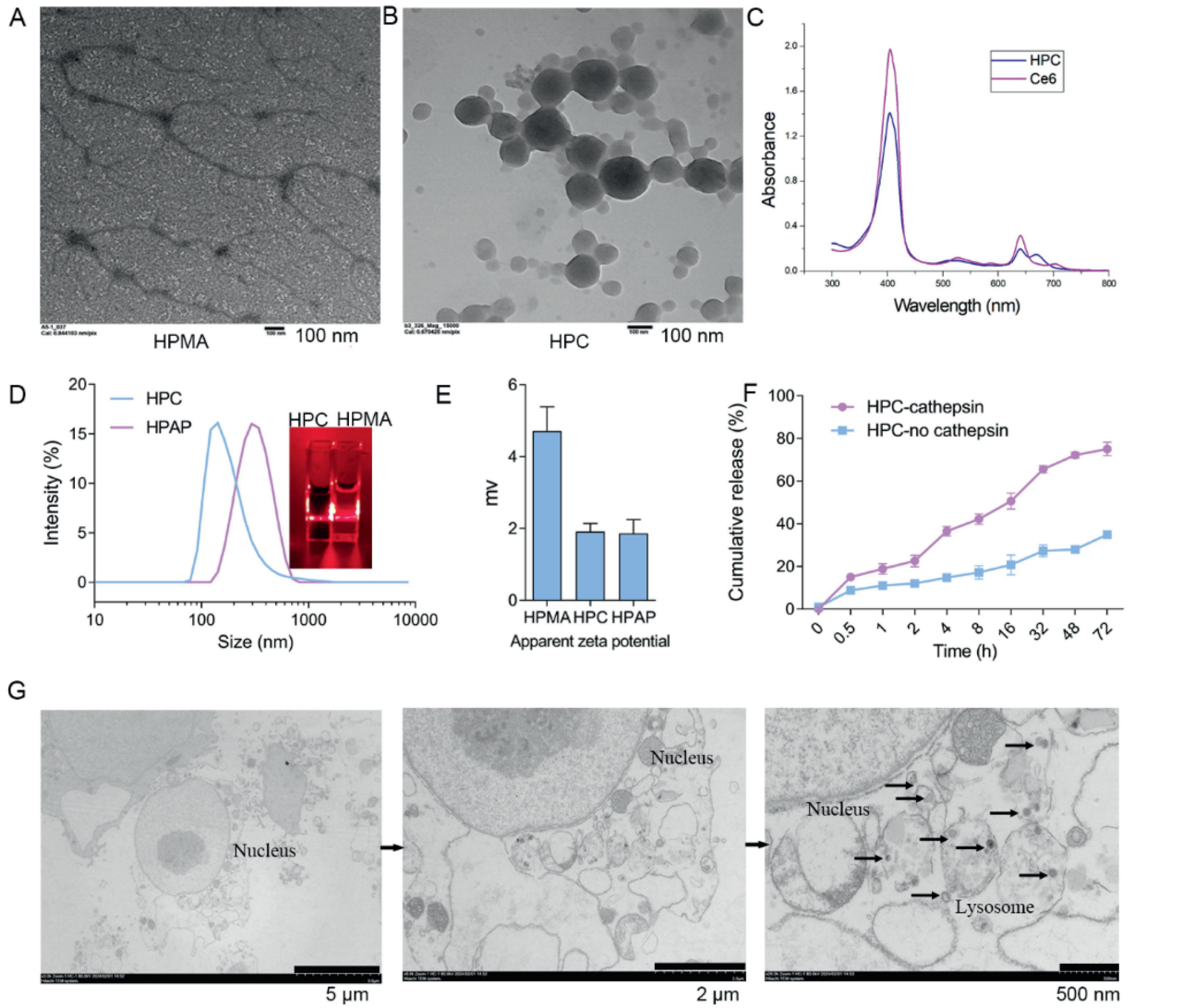

Figure 2 Characterization of nanomaterials *ex vivo*. (A) Sizes of HPMA nanoparticles observed under TEM. Scale bar = 100 nm. (B) Sizes of HPC nanoparticles observed under TEM. Scale bar = 100 nm. (C) Full-wavelength scan of HPC and Ce6 by UV−visible spectrophotometry. (D) The particle size of HPC and HPAP. (E) Sizes of potentials tested for HPMA, HPC, and HPAP. (F) Drug release of HPC in PBS with or without cathepsin; (G) Validation of HPAP targeting intracellular lysosomes.

significantly reduced the expression of PD-L1 on the cell membrane (Fig. 4D and E).

To evaluate the degradation of PD-L1 protein on the cell membrane, the expression of PD-L1 was evaluated by treating cells with different nanoparticles with 5 μmol/L HPAP, (0.5 μmol/L HPC+5 μmol/L HPAP)-dark and (0.5 μmol/L HPC+5 μmol/L HPAP)-light, respectively. The results showed that (0.5 μmol/L HPC+5 μmol/L HPAP)-light exhibited stronger degradation of PD-L1. Even in the presence of lysosome inhibitors under photo-irradiation conditions (0.5 μmol/L HPC+5 μmol/L HPAP)-light, the protein degradation of PD-L1 was minimal. The findings suggest that inhibition of lysosomal function is beneficial in reducing PD-L1 degradation (Fig. 4F and G). Concurrently, mRNA expression analysis of proteins post-degradation was performed using RT-qPCR (Supporting Information Fig. S6A and S6B). Next, we conducted a detailed exploration of the impact of polymer HPAP on the degradation of PD-L1 at concentrations of 2.5, 5, and 10 μmol/L. The findings revealed a conspicuous concentration-dependent degradation effect (Fig. 4H and I). Concurrently, an investigation into the time-dependent degradation trend of PD-L1 by HPAP was conducted (Supporting Information Fig. S7A and S7B). These results indicate that HPC, irrespective of light exposure, failed to elicit any degradation effect on PD-L1. In contrast, HPAP exhibited a notably concentration-dependent capacity for PD-L1 degradation. Furthermore, when cells were subjected to combined treatment with HPC and HPAP, a more pronounced induction of PD-L1 degradation was observed under light conditions. The full membrane results of the protein imprinting are provided in Supporting Information Fig. S8A and S8B.

3.5. *In vitro immune induction of ICD*

Ce6 is a frontline chemotherapeutic agent for numerous malignant tumors and an effective inducer of ICD[37]. Subsequently, the potential of the HPC to induce ICD in 4T-1 cells was investigated. ICD is characterized by the upregulation of calreticulin (CRT)

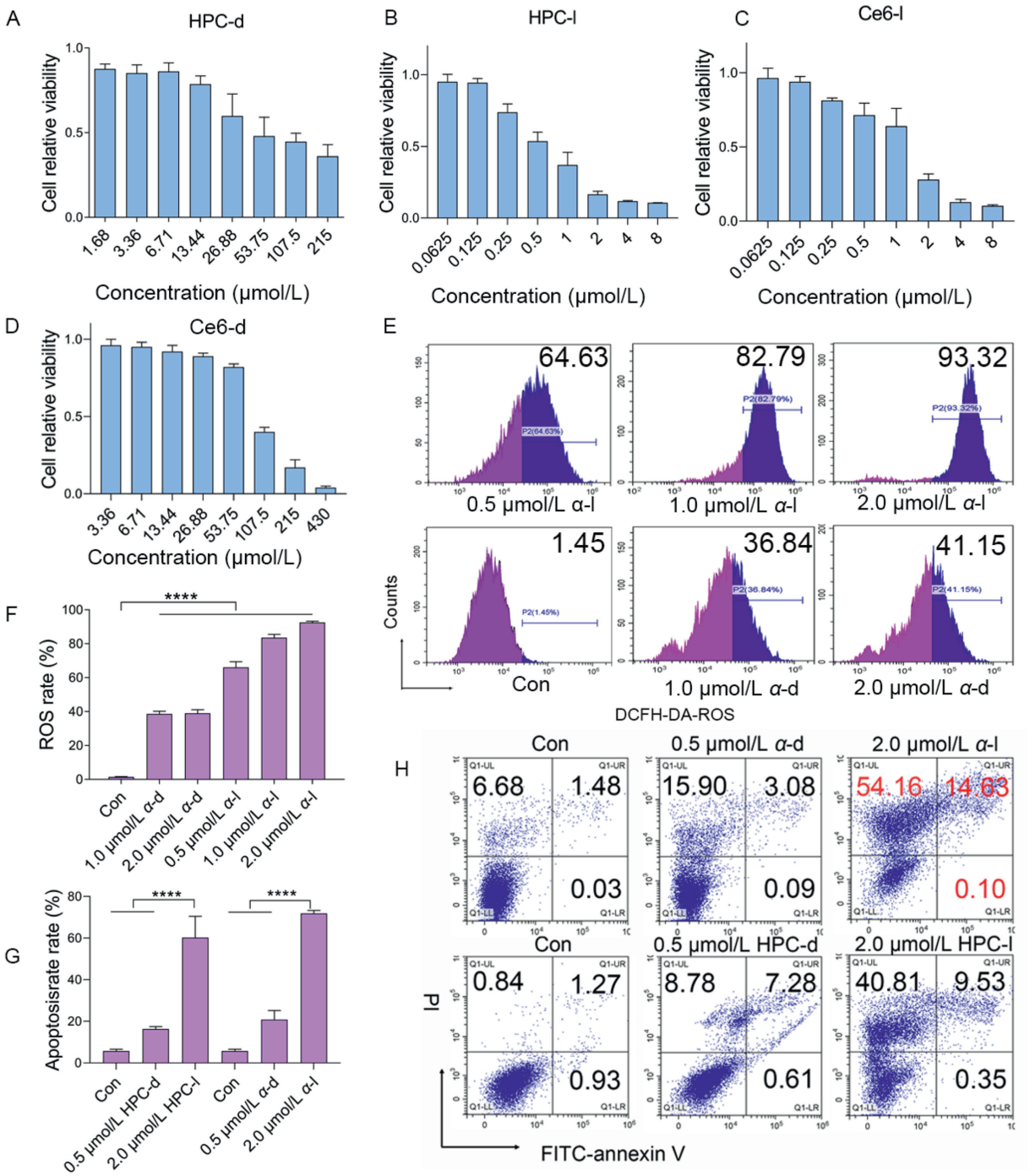

Figure 3 *In vitro* activity testing of nano drug delivery systems. (A) The IC_{50} of the HPC-dark is 70.03 μmol/L. (B) Phototoxicity assessment of compound HPC, exhibiting a phototoxicity of 0.62 μmol/L. (C) Phototoxicity evaluation of Ce6, with a phototoxicity of 1.13 μmol/L. (D) The IC_{50} of the Ce6-dark is 98.83 μmol/L. (E) ROS production under light and dark conditions for varying concentrations of HPC. (F) Columnar representation of ROS production under light and dark conditions for varying concentrations of HPC. (G) Columnar analysis depicting cell apoptosis effects of HPC + HPAP and HPC at different concentrations. (H) Experimental results of cell apoptosis at varying concentrations of HPC + HPAP. α represents the combination of HPC and HPAP, l represents light and d represents dark. Data are presented as mean ± SD ($n = 3$). The P values were calculated by ANOVA with Tukey's test. $^{**}P < 0.01$, $^{***}P < 0.001$, $^{****}P < 0.0001$.

expression on the cell membrane, extracellular release of high mobility group box 1 (HMGB1), and generation of adenosine triphosphate (ATP). CRT, HMGB1, and ATP play critical roles in antigen presentation and signaling to DC cells. Initially, we evaluated the expression of CRT protein on the 4T-1 cell surface after treatment with HPC and HPAP for 24 h. The results showed that the (HPC + HPAP)-light treatment group exhibited a 4.3-fold increase in CRT protein expression compared to the control group while exhibiting a 1.3-fold increase compared to the (HPC + HPAP)-dark treatment group (Fig. 5A and B). Similarly,

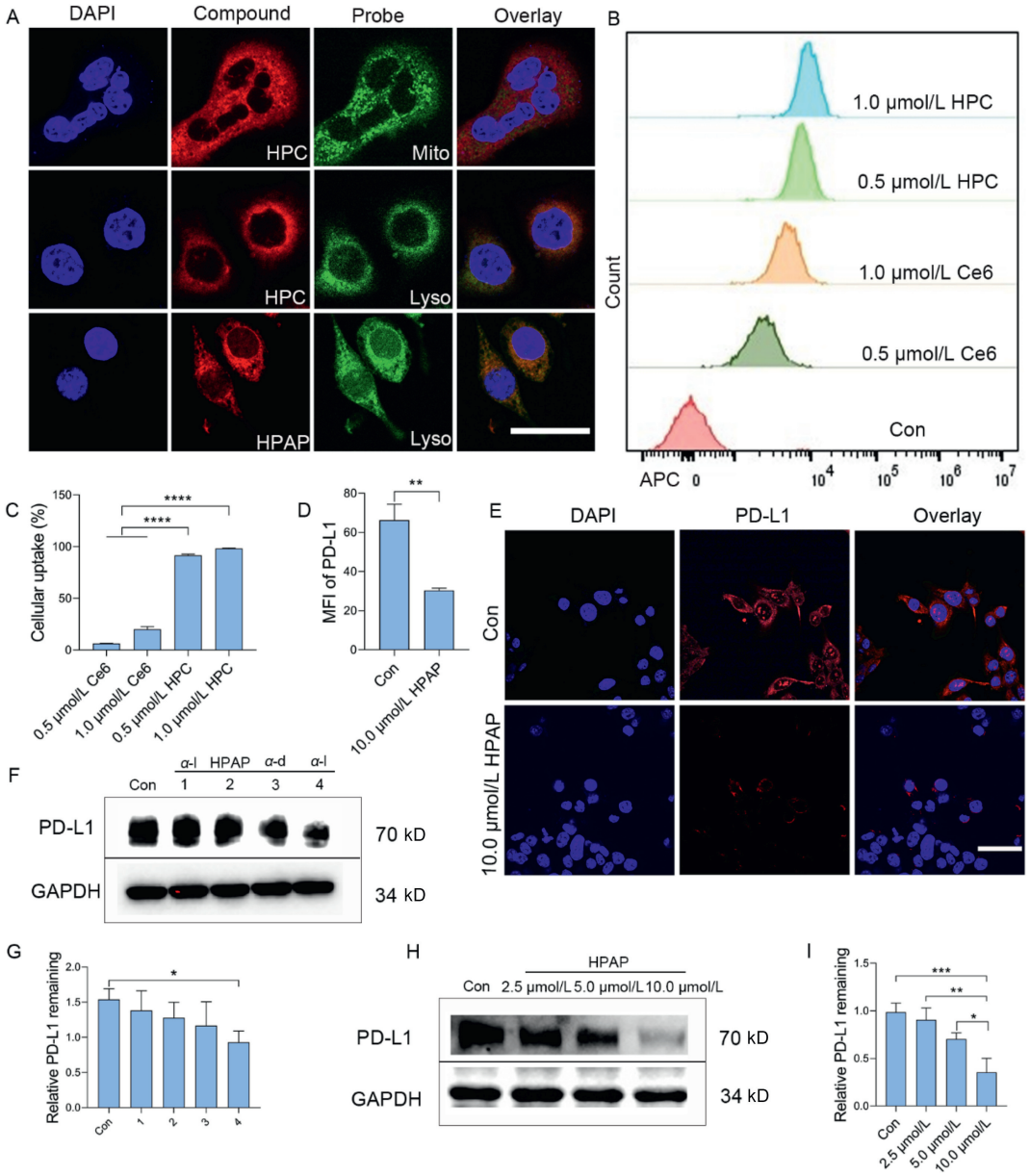

Figure 4 Cellular uptake and protein expression of nanomaterials. (A) Subcellular localization of lysosomes and mitochondria in cells upon uptake of HPC and HPAP. Scale bar = 50 μm. (B) Flow cytometric analysis of cell uptake for HPC and Ce6. (C) Flow cytometry analysis of cellular uptake statistics of HPC and Ce6. (D) The column analysis of confocal microscopy for degradation of PD-L1 by treated with 10 μmol/L HPAP. (E) Confocal observation of the degradation of HPAP pairs of PD-L1 proteins. Scale bar = 50 μm. (F) Western blotting analysis of degradation of PD-L1. 1 represents lysosomal inhibitors and (0.5 μmol/L HPC+5 μmol/L HPAP)-light. 2 represents 5 μmol/L HPAP. 3 represents (5 μmol/L HPAP+0.5 μmol/L HPC)-dark. 4 represents (5 μmol/L HPAP+0.5 μmol/L HPC)-light. (G) Column graph analysis of PD-L1 protein expression detected by Western blotting in different treatment groups. (H) Western blotting results of PD-L1 protein expression after treatment with different concentrations of HPAP. (I) The column analysis results for the degradation of PD-L1 protein by treatment with different concentrations of HPAP. α represents the combination of HPC and HPAP, l represents light and d represents dark. Data are presented as mean ± SD ($n = 3$). ANOVA calculated the P values with Tukey's test or t-test. *$P < 0.05$, **$P < 0.01$.

after treatment with HPC and HPAP for 24 h, cell supernatant was collected to assess the release of ATP and HMGB1. The (HPC + HPAP)-light treatment group exhibited a 42-fold increase in ATP release compared to the control group and a 2-fold increase compared to the (HPC + HPAP)-dark treatment group (Fig. 5C). In comparison to the control group, the (HPC + HPAP)-light treatment group demonstrated a 7.2-fold elevation in HMGB1 release, while a 2.4-fold increase was observed compared to the (HPC + HPAP)-dark treatment group (Fig. 5D). These convincing results confirmed the specific characteristics of ICD induced by (HPC + HPAP)-light in 4T-1 cells.

To verify the induction of immune factors *in vitro*, inflammatory factors IL-6, TNFα, and IFN-γ were further investigated[38], The 4T-1 and RAW264.7 cell lines were treated separately with

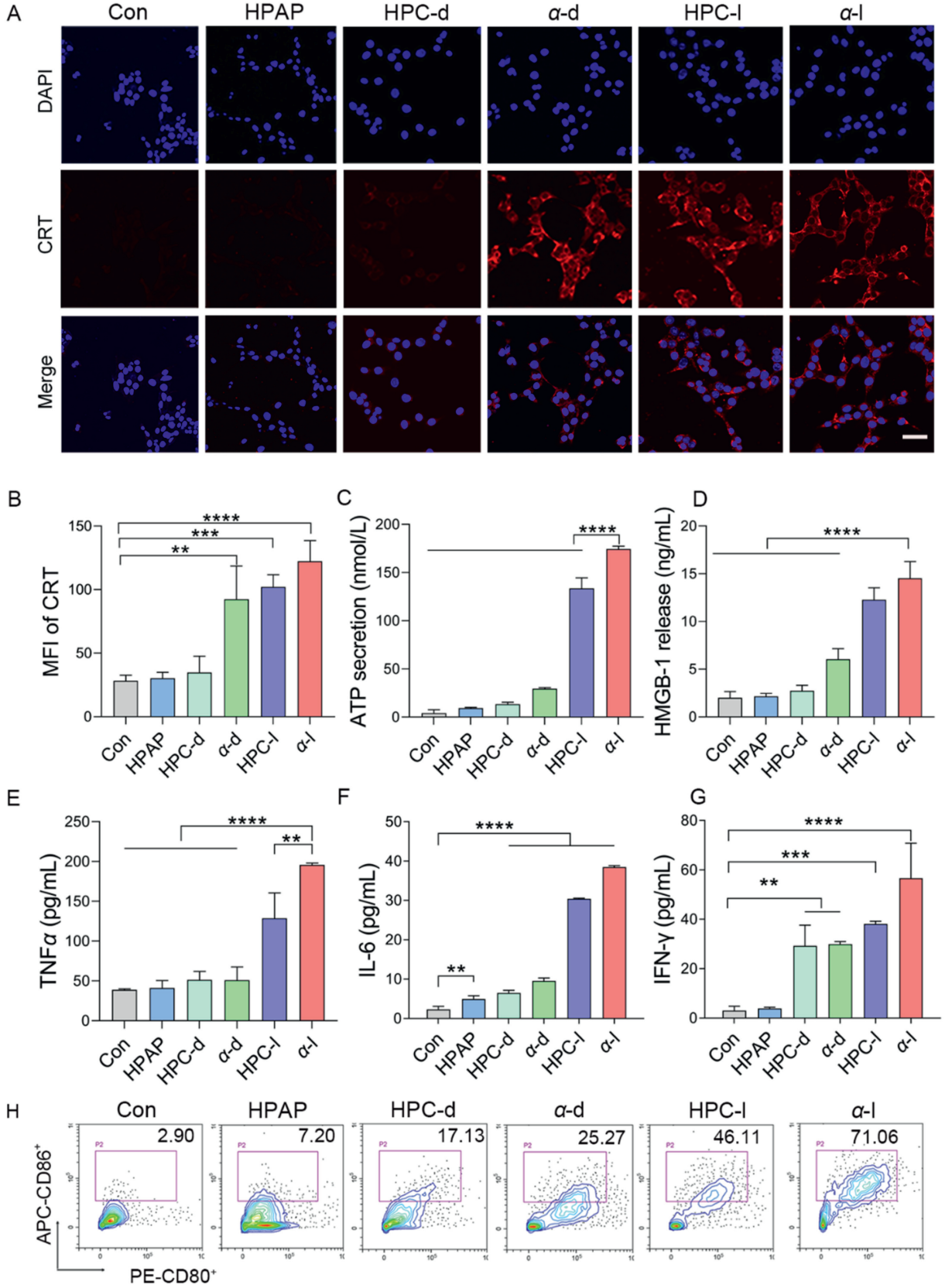

Figure 5 *In vitro* immune induction expression testing. (A) CRT in different experimental groups. Scale bar = 50 μm. (B) Columnar analysis depicting CRT induction in different experimental groups. (C) Intracellular ATP release post-administration of treatments. (D) Expression analysis of secreted HMGB-1 protein in cells after treatment administration. (E) *In vitro* TNFα expression profiles in different treatment groups. (F) *In vitro* IL-6 expression patterns in different treatment groups. (G) *In vitro* IFN-γ expression profiles in different treatment groups. (H) Analysis of the *in vitro*-induced maturation outcomes of DCs. α represents the combination of HPC and HPAP, l represents light and d represents dark. Data are presented as mean ± SD ($n = 3$). The P values were calculated by ANOVA with Tukey's test. *$P < 0.05$, **$P < 0.01$, ***$P < 0.001$, ****$P < 0.0001$.

the HPAP and HPC at a concentration of 0.5 μmol/L, and with a combination of HPC with HPAP for 24 h. Subsequently, the expression levels of immune factors were measured using high-sensitivity enzyme-linked immunosorbent assay (ELISA) kits for mouse IL-6, TNFα, and IFN-γ. The expression of TNFα in the (HPC + HPAP)-light treatment group reached as high as 195.65 pg/mL (Fig. 5E). The results indicated that in the combination (HPC + HPAP)-light group, the expression level of IL-6 reached 38.46 pg/mL (Fig. 5F), and that of IFN-γ reached 56.64 pg/mL (Fig. 5G). These findings suggest that (HPC + HPAP)-light could significantly induce high expression levels of the cellular immune factors mouse TNFα, IL-6, and IFN-γ. Finally, the verification of DCs maturation *in vitro* revealed that (HPC + HPAP)-light effectively induced maturation by up to 71.06% (Fig. 5H and Supporting Information Fig. S9).

3.6. *Evaluation of anti-tumor effects in vivo*

Effective tumor targeting is pivotal for exerting inhibitory effects on tumors. To validate the targeting capability of HPC and HPAP, *in vivo* live imaging was performed. The results revealed that free Ce6 was predominantly distributed in the mouse brain and tumor regions, while HPC and the combination of HPC + HPAP were primarily concentrated within the tumors, with lower accumulation in other regions (Fig. 6A). The results of organ imaging showed that HPC and HPAP were mainly concentrated in the tumor tissues, and the metabolism mainly occurred in liver and kidneys after 4 h of administration (Fig. 6B). Next, to assess the biosafety of HPC and HPAP, the 4T1 tumor isograft model was employed for *in vivo* pharmacological experiments. BALB/c mice were provided by the Center for Translational Medicine

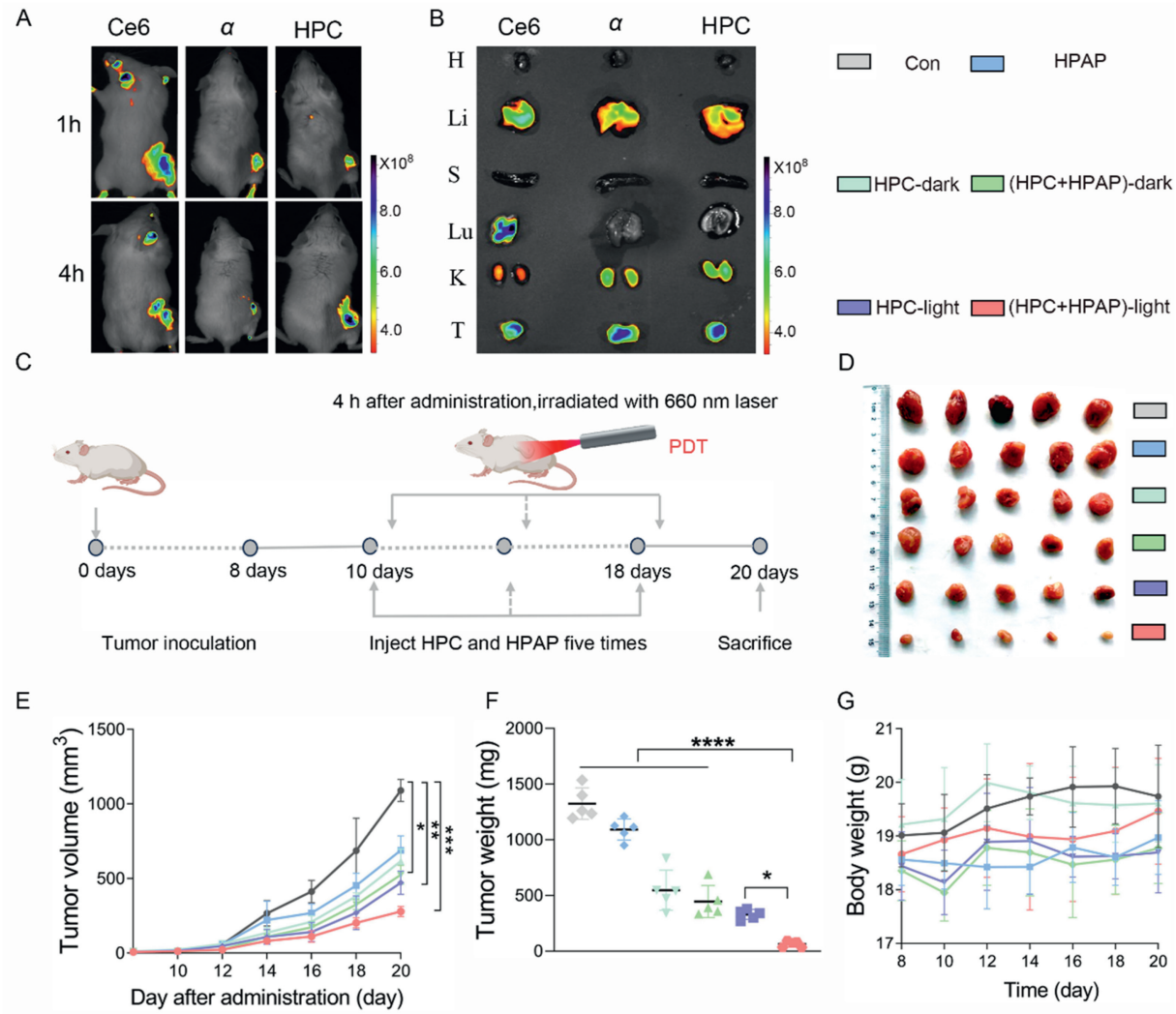

Figure 6 *In vivo* anti-tumor activity research results. (A) *In vivo* imaging results of Ce6, HPC, and (HPC + HPAP) after intravenous injection in mice. (B) Fluorescence photographs of heart, liver, spleen, lung, kidney, and tumor in different groups. H: heart, Li: liver, S: spleen, Lu: lung, K: kidney, T: tumor. (C) The treatment plan for tumor-bearing mice after HPC and HPAP tail vein administration. (D) Visual representation of tumor sizes in different groups. (E) Curved diagram illustrating the volume growth of tumors in each group. (F) Test results of the tumor weight. (G) Statistical graph depicting body weights. α represents the combination of HPC and HPAP, l represents light and d represents dark. Data are presented as mean ± SD ($n = 5$). The P values were calculated by one-way ANOVA with Tukey's test or two-way ANOVA. *$P < 0.05$, **$P < 0.01$, ***$P < 0.001$, ****$P < 0.0001$.

Experimental Animal Research at Shanghai University. When the tumor volume reached approximately 100 mm^3, mice were randomly divided into 6 groups, including one control group and five experimental groups, each consisting of 5 mice. The five treatment groups were administered a complex of HPC and HPAP *via* tail vein injection, with HPC at a dose of 5 mg/kg and HPAP at 8 mg/kg. The treatment regimen for BALB/c tumor-bearing mice was illustrated in Fig. 6C. Photographic documentation of tumor sizes in each group was presented in Fig. 6D, revealing that (HPC + HPAP)-light treatment exhibited a superior tumor growth inhibitory effect relative to other treatment groups (Fig. 6E). Following 5 administrations, the tumor weights for each group were subjected to statistical analysis, concurrently assessing the therapeutic effects of the drugs on the tumors. The analysis results revealed that the (HPC + HPAP)-light treatment demonstrated a superior inhibitory effect on tumor growth compared to other treatment groups (Fig. 6F). Subsequently, 12 days post-treatment, blood and organs were collected from each group of mice for physicochemical analysis. The results revealed that the mouse body weight fluctuated around 19 g after 5 consecutive administrations, exhibiting no significant difference from the physiological saline group, indicating negligible systemic toxicity induced by the nanoparticles at this dosage (Fig. 6G).

3.7. *Evaluation of protein degradation and ICD induction in vivo*

Simultaneously, an assessment of PD-L1 degradation in tumors across different groups revealed that the (HPC + HPAP)-light treatment group displayed more effective PD-L1 degradation compared to the other groups (Fig. 7A and C). To verify the *in vivo* immune induction effect during the drug administration, the expression levels of HMGB1 and CRT in the tumors were evaluated. (HPC + HPAP)-light group exhibited higher levels of early *in vivo* expression of HMGB1 (Fig. 7B and D) and CRT (Fig. 7E and F) compared to the other groups. Immunohistochemistry expression level assessments also revealed that relative to the other groups, the (HPC + HPAP)-light treatment group demonstrated higher levels of early *in vivo* expression of CRT and HMGB1 (Supporting Information Fig. S10A and S10B).

3.8. *Immune factor induction and immune activation in vivo*

Subsequently, Ki67 and H&E staining were performed to assess the tumor cell proliferation and apoptosis in each group of mice after the late-stage treatment (Fig. 8A). The (HPC + HPAP)-light group exhibited fewer Ki67-positive cells and more apoptotic

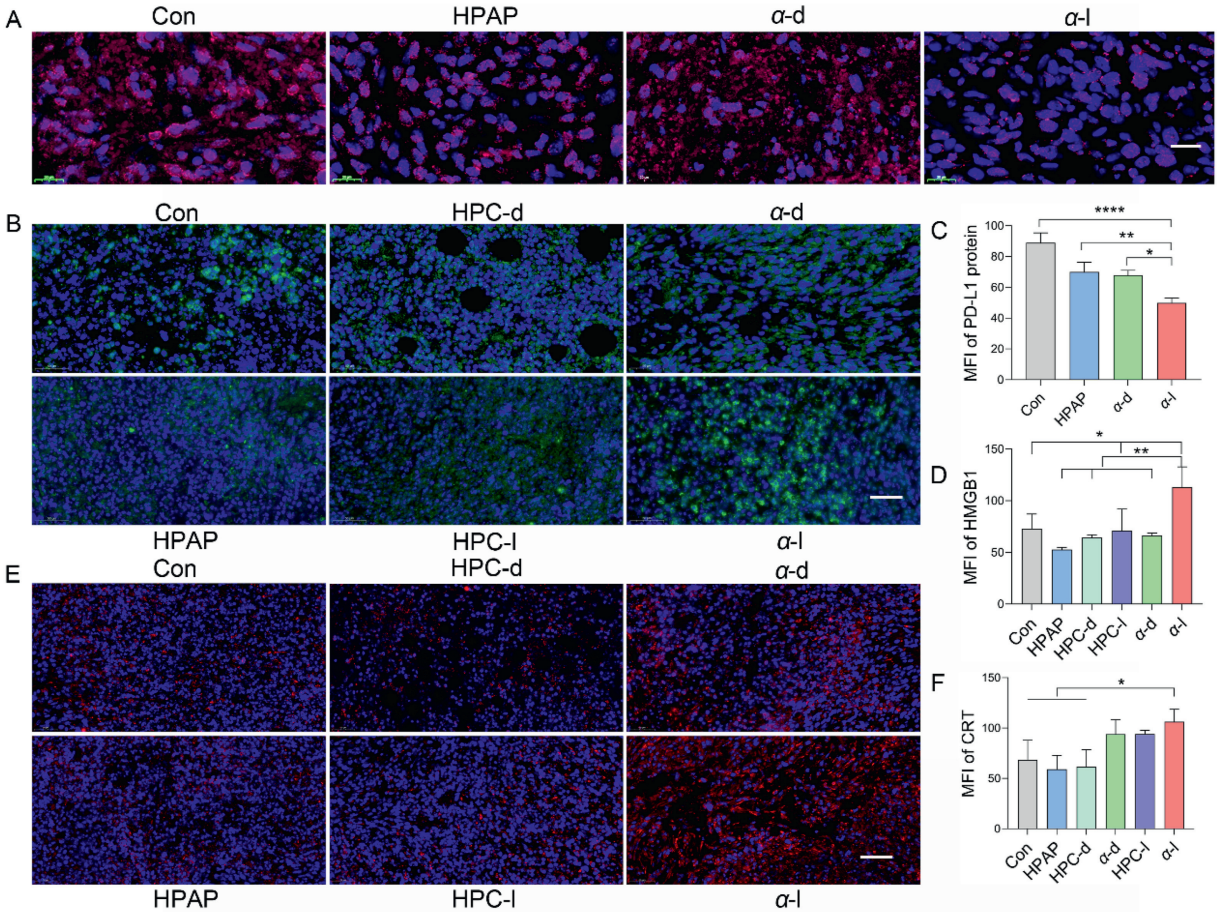

Figure 7 *In vivo* testing of protein degradation and immune induction results. (A) Fluorescence staining images of PD-L1 degradation in tumors across various groups. Scale bar = 20 μm. (B) The expression of HMGB1 protein in various tumor groups. Scale bar = 50 μm. (C) Fluorescence histograms of PD-L1 degradation in various tumor subtypes. (D) Fluorescence quantification of HMGB1 in different tumor subtypes. (E) The expression status of CRT in various tumor groups. (F) The statistical results of CRT for each group. Scale bar = 50 μm. α represents the combination of HPC and HPAP, l represents light and d represents dark. Data are presented as mean ± SD ($n = 3$). The P values were calculated by one-way ANOVA with Tukey's test or two-way ANOVA. *$P < 0.05$, **$P < 0.01$, ***$P < 0.001$, ****$P < 0.0001$.

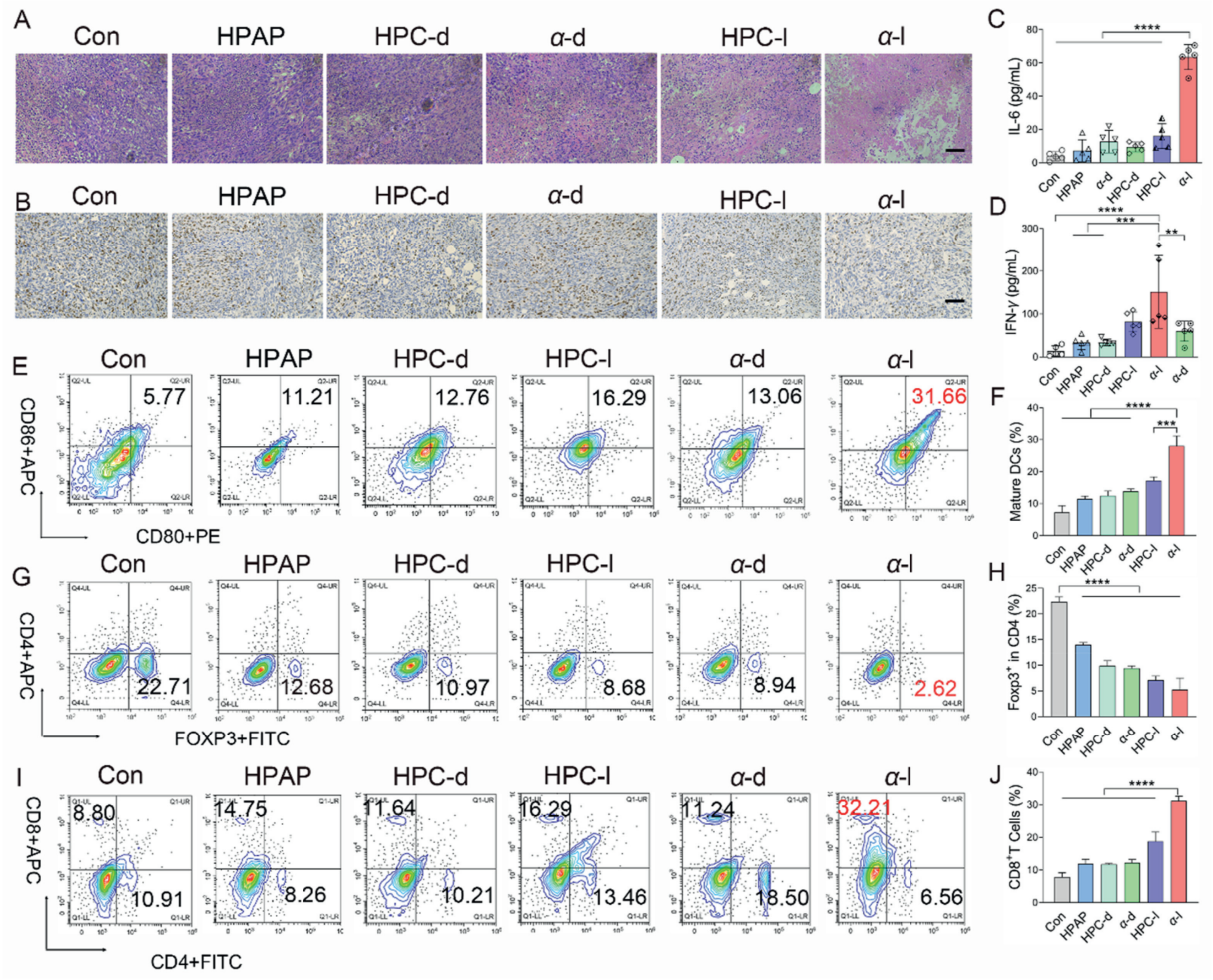

Figure 8 Evaluation of drug efficacy against tumors. (A) H&E staining images illustrating tumor sizes in each group. Scale bar = 50 μm. (B) Staining images showing Ki67 expression in tumors from various groups. Scale bar = 50 μm. (C) Test results for the immune factor IL-6 in peripheral blood. Data are presented as mean ± SD (n = 5). (D) Test results for the immune factor INF-γ in peripheral blood. Data are presented as mean ± SD (n = 5). (E) Flow cytometry results display the expression of induced DCs within mice lymph nodes. (F) Statistical analysis of induced DCs within mouse lymph nodes. (G) Flow cytometry statistics of Tregs expression within tumors. (H) Statistical findings of induced Tregs expression within tumors. (I) Flow cytometry statistics of $CD4^+$ and $CD8^+$ expression within tumors. (J) Statistical results of $CD4^+$ and $CD8^+$ expression within tumors. α represents the combination of HPC and HPAP, l represents light and d represents dark. Data are presented as mean ± SD (n = 3). The P values were calculated by one-way ANOVA with Tukey's test $^*P < 0.05$, $^{**}P < 0.01$, $^{***}P < 0.001$, $^{****}P < 0.0001$.

cells, confirming the enhanced tumor growth inhibition in the (HPC + HPAP)-light treatment group (Fig. 8B). Due to the crucial role of immune-related cytokines, represented by mouse TNFα, IFN-γ, and IL-6, in promoting cytotoxic T cell-mediated killing, an *in vivo* immune factor test was conducted[39,40]. Peripheral blood from mice treated with different nanoparticles was collected for cytokine analysis using a mouse TNFα, IL-6, and IFN-γ high-sensitivity ELISA kit. The results revealed that when HPC and HPAP were administered individually, the expression levels of immune factors TNFα, IL-6, and IFN-γ were relatively low. However, under light conditions, the expression levels of TNFα, IL-6, and IFN-γ induced by the polymer HPC showed a slight increase. Under (HPC + HPAP)-light conditions, the IL-6 immune factor level increased to 57.51 pg/mL (Fig. 8C), and the IFN-γ immune factor level reached 151.60 pg/mL (Fig. 8D). The TNFα expression level in the (HPC + HPAP)-light group reached 170.01 pg/mL (Supporting Information Fig. S11). This indicates that, under light conditions, the HPC and HPAP could significantly induce the production of immune factors TNFα, IL-6, and IFN-γ. The elevated expression of TNFα, IL-6, and IFN-γ could stimulate the proliferation of immune response cells, enhance antigen presentation, increase the activity of immune cells, and promote $CD8^+$ T cell-mediated killing of tumor cells.

To gain further insight into potential mechanisms underlying immune enhancement, mature DCs were collected from tumor-draining lymph nodes, and their maturation status was analyzed using flow cytometry across various treatment groups. The experimental findings revealed that the proportion of mature DCs ($CD80^+/CD86^+$) was approximately 31.66% in the (HPC + HPAP)-light group, which was 5.5 times that of mature DCs (5.77%) in the lymph nodes of control-treated mice. In contrast, in the HPC-light and HPAP treatment groups, the proportions of mature DCs ($CD80^+/CD86^+$) in mice lymph nodes were approximately 16.29% and 11.21%, respectively (Fig. 8E

and F). Additionally, the expression of immunosuppressive $Foxp3^+$ regulatory T cells (Tregs) in murine tumor tissue was further evaluated. The number of Tregs cells was 22.71% in the control group, whereas the quantity of Tregs cells was merely 2.62% in the tumor tissue treated with (HPC + HPAP)-light. These results suggested a significant decrease in the population of helper immune T cells in the (HPC + HPAP)-light group (Fig. 8G and H). (HPC + HPAP)-light could effectively activate T lymphocytes, facilitate the conversion of $CD8^+$ T cells into memory T cells, and induce a robust adaptive immune response. The proportion of $CD8^+$ T cells soared to 32.21%, which was 3.6 times that of the control group. In the HPC-light and HPAP treatment groups, the proportions of $CD8^+$ T cells in mouse tumors were 16.29% and 14.75%, respectively (Fig. 8I and J). Overall, (HPC + HPAP)-light demonstrated the capability to efficiently activate a systemic anti-tumor immune response, reshape the tumor's immune-suppressive microenvironment, and possess enduring immune memory protection ability.

Finally, major organs, including the heart, liver, spleen, lung, and kidney, from mice subjected to various drug treatments were subjected to H&E staining and captured under a fluorescence microscope (Supporting Information Fig. S12). The results indicated that the main organ tissues of the treated mice exhibited no notable morphological changes compared to those of mice treated with physiological saline, demonstrating the favorable biocompatibility of HPC and HPAP in treating mice.

4. Conclusions

In summary, we designed and synthesized a novel peptide-polymer system susceptible to cathepsin cleavage for the delivery of the photosensitizer Ce6 and PD-L1 peptide antagonists. HPC undergoes endocytosis into cells and is cleaved to release the antitumor agent Ce6, exerting a synergistic effect of ICD and PDT. HPAP facilitates the cross-linking and internalization of PD-L1 on the membrane, promoting its degradation within lysosomes. The combined therapy of HPC and HPAP offers a versatile approach, reshaping the "cold" tumor immune microenvironment and enhancing the immune system's cytotoxicity against tumors. Additionally, the polymer strategy enhances the tumor-targeting effect of the photosensitizer Ce6, reducing damage to normal tissues. Furthermore, HPAP provides a novel example of receptor crosslinking-mediated internalization and lysosomal degradation of PD-L1. We effectively combined the effects of ICD, PD-L1 degradation, and photodynamic therapy in triple-negative breast cancer tumor models, offering new insights into tumor immunotherapy.

However, compared to similar designs, although our strategy demonstrates significant advantages in PD-L1 degradation efficiency and material biocompatibility[41,42], translating this design from the laboratory to clinical application still faces several challenges. First, ensuring the safety and minimizing potential side effects of the technology is paramount. Despite the polymer's excellent performance in enhancing targeting specificity, its long-term safety profile and potential immunogenic responses necessitate further research and validation. Second, evaluating clinical efficacy and addressing individual variability among patients are crucial considerations, requiring broad clinical trials to validate effectiveness and reproducibility.

Despite these challenges, we believe our multifunctional PD-L1 regulation and drug delivery system holds promise as a pivotal tool in future cancer therapy, providing more effective treatment options for patients. As ongoing research and clinical trials progress, we anticipate continued development and widespread adoption of these technologies in practical healthcare settings.

Acknowledgments

This work was supported by the National Natural Science Foundation of China (No. 22077078 to Honggang Hu, 22107062 to Fei Gao), the National Key Research and Development Program of China (No. 2021YFC2100201 to Honggang Hu), and the Shanghai Rising-Star Program (No. 23QA1403500 to Shipeng He, China).

Author contributions

Changyong Guo: Writing − original draft, Project administration, Investigation, Formal analysis, Data curation. Shipeng He: Writing − review & editing, Project administration, Investigation, Funding acquisition, Conceptualization. Huaxing Shen: Formal analysis, Data curation. Wei Cong: Formal analysis. Jinqiu Li: Investigation, Formal analysis. Yajing Ji: Data curation. Wenjing Huang: Investigation. Fei Gao: Writing − review & editing, Investigation, Funding acquisition. Honggang Hu: Writing − review & editing, Funding acquisition, Conceptualization.

Conflicts of interest

The authors have no conflicts of interest to declare.

Appendix A. Supporting information

Supporting Information to this article can be found online at https://doi.org/10.1016/j.apsb.2025.05.022.

References

1. Schreiber RD, Old LJ, Smyth MJ. Cancer immunoediting: integrating immunity's roles in cancer suppression and promotion. *Science* 2011; **331**:1565−70.
2. Boussiotis VA. Molecular and biochemical aspects of the PD-1 checkpoint pathway. *N Engl J Med* 2016;**375**:1767−78.
3. Bao R, Wang Y, Lai J, Zhu H, Zhao Y, Li S, et al. Enhancing anti-PD-1/PD-L1 immune checkpoint inhibitory cancer therapy by CD276-targeted photodynamic ablation of tumor cells and tumor vasculature. *Mol Pharm* 2019;**16**:339−48.
4. Shi C, Wang Y, Wu M, Chen Y, Liu F, Shen Z, et al. Promoting antitumor immunity by targeting TMUB1 to modulate PD-L1 polyubiquitination and glycosylation. *Nat Commun* 2022;**13**:6915.
5. Wang H, He ZX, Gao YJ, Feng DX, Wei XD, Huang YH, et al. Dual-pronged attack: pH-driven membrane-anchored NIR dual-type nanophotosensitizer excites immunogenic pyroptosis and sequester immune checkpoint for enhanced prostate cancer photo-immunotherapy. *Adv Sci* 2023;**10**:202302422.
6. Bordon Y. Combining EZH2 inhibition with senescence induction helps immune cells fight pancreatic cancer. *Nat Rev Immunol* 2023;**23**:411.
7. Mills KHG. Innate lymphoid cells recruit T cells to turn up the heat on tumors. *Cancer Cell* 2022;**40**:362−4.
8. Moldvay J, Rojkó L, Téglási V, Fábián K, Pipek O, Vágvölgyi A, et al. P2.04-08 platinum-based chemotherapy is associated with altered PD-L1 expression in lung cancer. *J Thorac Oncol* 2018;**13**:S733.
9. Ge Y, Wang HY, Ren JH, Liu WL, Chen LJ, Chen HQ, et al. Oncolytic vaccinia virus delivering tethered IL-12 enhances antitumor effects with improved safety. *J Immunother Cancer* 2020;**8**:e000710.

10. Yang WJ, Zhu GZ, Wang S, Yu GC, Yang Z, Lin LS, et al. *In situ* dendritic cell vaccine for effective cancer immunotherapy. *ACS Nano* 2019;**13**:3083−94.
11. Zeng Y, Zhao LF, Li K, Ma JW, Chen D, Liu CH, et al. Aptamer-functionalized nanoplatforms overcoming temozolomide resistance in synergistic chemo/photothermal therapy through alleviating tumor hypoxia. *Nano Res* 2023;**16**:9859−72.
12. Zhang R, Zhu ZY, Lv HY, Li FT, Sun SQ, Li J, et al. Immune checkpoint blockade mediated by a small-molecule nanoinhibitor targeting the PD-1/PD-L1 pathway synergizes with photodynamic therapy to elicit antitumor immunity and antimetastatic effects on breast cancer. *Small* 2019;**15**:1903881.
13. Jiao QS, Zheng YX, Xie QQ, Luo X, Zhou SY, Pei SC, et al. A dual-responsive morphologically-adaptable nanoplatform for targeted delivery of activatable photosensitizers in precision photodynamic therapy. *Small* 2023;**20**:202309054.
14. Zhou JY, Shen QH, Hong XJ, Zhang WY, Su Q, Li WG, et al. Synergization of an endoplasmic reticulum-targeted iridium(III) photosensitizer with PD-L1 inhibitor for oral squamous cell carcinoma immunotherapy. *Chem Eng J* 2023;**474**:145516.
15. Huang SX, Ding DB, Lan TY, He GH, Ren JN, Liang RP, et al. Multifunctional nano drug performs son dynamic therapy and inhibits TGF-β to boost the immune response against colorectal cancer and liver metastasis. *Acta Biomater* 2023;**164**:538−52.
16. Li YG, Zhang PZ, Xie YJ, Yang JP, Yang YQ, Shi LL, et al. Photosensitizers with multiple degradation modes for efficient and post-operatively safe photodynamic therapy. *Biomaterials* 2023;**299**: 122182.
17. Jin FY, Qi J, Liu D, You YC, Shu GF, Du Y, et al. Cancer-cell-biomimetic upconversion nanoparticles combining chemo-photodynamic therapy and CD73 blockade for metastatic triple-negative breast cancer. *J Control Release* 2021;**337**:90−104.
18. Zhou ML, Luo CH, Zhou Z, Li L, Huang Y. Improving anti-PD-L1 therapy in triple-negative breast cancer by polymer-enhanced immunogenic cell death and CXCR4 blockade. *J Control Release* 2021;**334**: 248−62.
19. Lu ZR, Kopecková P, Kopecek J. Polymerizable fab' antibody fragments for targeting of anticancer drugs. *Nat Biotechnol* 1999;**17**: 1101−4.
20. Wang JW, Li L, Yang JY, Clair PM, Glenn MJ, Stephens DM, et al. Drug-free macromolecular therapeutics induce apoptosis in cells isolated from patients with B cell malignancies with enhanced apoptosis induction by pretreatment with gemcitabine. *Nanomedicine* 2019;**16**: 217−25.
21. Li L, Li YC, Yang CH, Radford DC, Wang JW, Janát-Amsbury M, et al. Inhibition of immunosuppressive tumors by polymer-assisted inductions of immunogenic cell death and multivalent PD-L1 cross-linking. *Adv Funct Mater* 2020;**30**:1908961.
22. Zhang LB, Zhang R, Yang JY, Wang JW, Kopeček JD. Indium-based and iodine-based labeling of HPMA copolymer-epirubicin conjugates: impact of structure on the *in vivo* fate. *J Control Release* 2016;**235**: 306−18.
23. Satchi-Fainaro R, Puder M, Davies JW, Tran HT, Sampson DA, Greene AK, et al. Targeting angiogenesis with a conjugate of HPMA copolymer and TNP-470. *Nat Med* 2004;**10**:255−61.
24. Wang HB, Yao H, Li CS, Shi HB, Lan J, Li ZL, et al. HIP1R targets PD-L1 to lysosomal degradation to alter T cell-mediated cytotoxicity. *Nat Chem Biol* 2019;**15**:42−50.
25. Burr ML, Sparbier CE, Chan YC, Williamson JC, Woods K, Beavis PA, et al. CMTM6 maintains the expression of PD-L1 and regulates anti-tumour immunity. *Nature* 2017;**549**:101−5.
26. Li L, Sun W, Zhong JJ, Yang QQ, Zhu X, Zhou Z, et al. Multistage nanovehicle delivery system based on stepwise size reduction and charge reversal for programmed nuclear targeting of systemically administered anticancer drugs. *Adv Funct Mater* 2015;**25**:4101−13.
27. Pike DB, Ghandehari H. HPMA copolymer−cyclic RGD conjugates for tumor targeting. *Adv Drug Deliv Rev* 2010;**62**:167−83.
28. Pasut G, Veronese FM. Polymer−drug conjugation, recent achievements and general strategies. *Prog Polym Sci* 2007;**32**:933−61.
29. Yao H, Lan J, Li CS, Shi HB, Brosseau JP, Wang HB, et al. Inhibiting PD-L1 palmitoylation enhances T-cell immune responses against tumors. *Nat Biomed Eng* 2019;**3**:306−17.
30. Jiang X, Yi L, Li C, Wang HX, Xiong W, Li Y, et al. Mitochondrial disruption nanosystem simultaneously depressed programmed death ligand-1 and transforming growth factor-β to overcome photodynamic immunotherapy resistance. *ACS Nano* 2024;**18**:3331−48.
31. Yi L, Jiang X, Zhou ZG, Xiong W, Xue F, Liu Y, et al. A hybrid nanoadjuvant simultaneously depresses PD-L1/TGF-β*1* and activates cGAS−STING pathway to overcome radio-immunotherapy resistance. *Adv Mater* 2024;**36**:e2304328.
32. Liu Y, Zhou ZG, Hou JT, Xiong W, Kim HJ, Chen JS, et al. Tumor selective metabolic reprogramming as a prospective PD-L1 depression strategy to reactivate immunotherapy. *Adv Mater* 2022;**34**:2206121.
33. Zhou ZG, Li C, Li C, Zhou L, Tan S, Hou WB, et al. Mitochondria-targeted nanoadjuvants induced multi-functional immune-microenvironment remodeling to sensitize tumor radio-immunotherapy. *Adv Sci* 2024;**11**:2400297.
34. Nakada T, Masuda T, Naito H, Yoshida M, Ashida S, Morita K, et al. Novel antibody drug conjugates containing exatecan derivative-based cytotoxic payloads. *Bioorg Med Chem Lett* 2016;**26**:1542−5.
35. Chang HN, Liu BY, Qi YK, Zhou Y, Chen YP, Pan KM, et al. Blocking of the PD-1/PD-L1 interaction by a *D*-peptide antagonist for cancer immunotherapy. *Angew Chem Int Ed* 2015;**54**:11760−4.
36. Liu YL, Yang JX, Liu B, Cao W, Zhang JP, Yang YM, et al. Human iPS cells loaded with MnO_2-based nanoprobes for photodynamic and simultaneous enhanced immunotherapy against cancer. *Nano-Micro Lett* 2020;**12**:127.
37. He ZJ, Zhou H, Zhang Y, Du XY, Liu SG, Ji JB, et al. Oxygen-boosted biomimetic nanoplatform for synergetic phototherapy/ferroptosis activation and reversal of immune-suppressed tumor microenvironment. *Biomaterials* 2022;**290**:121832.
38. Li C, Qiu QJ, Gao X, Yan XY, Fan CZ, Luo X, et al. Sialic acid conjugate-modified liposomal platform modulates immunosuppressive tumor microenvironment in multiple ways for improved immune checkpoint blockade therapy. *J Control Release* 2021;**337**:393−406.
39. Chang MY, Wang M, Liu B, Zhong WB, Jana DB, Wang YF, et al. A cancer nanovaccine based on a FeAl-layered double hydroxide framework for reactive oxygen species-augmented metalloimmunotherapy. *ACS Nano* 2024;**18**:8143−56.
40. Fan DY, Liu XH, Ren YM, Luo ZH, Li YB, Dong J, et al. Harnessing antimicrobial peptide-coupled photosensitizer to combat drug-resistant biofilm infections through enhanced photodynamic therapy. *Acta Pharm Sin B* 2024;**14**:1759−71.
41. Zhou ZG, Chen JS, Liu Y, Zheng CJ, Luo WJ, Chen LL, et al. Cascade two-stage tumor re-oxygenation and immune re-sensitization mediated by self-assembled albumin-sorafenib nanoparticles for enhanced photodynamic immunotherapy. *Acta Pharm Sin B* 2022;**12**:4204−23.
42. Zhou ZG, Wang HX, Li J, Jiang X, Li ZP, Shen JL. Recent progress, perspectives, and issues of engineered PD-L1 regulation nano-system to better cure tumor: a review. *Int J Biol Macromol* 2024;**254**: 127911.